# Effect of energy variation on the dissipative evolution of the system in heavy-ion fusion reactions

N. K. Rai,* Vivek Mishra, and Ajay Kumar
*Department of Physics, Banaras Hindu University, Varanasi-221005, India*

(Received 8 June 2018; published 28 August 2018)

In heavy-ion fusion reactions, the energy of the projectile couples with the intrinsic degrees of freedom of the target during the collision process and this leads to a dissipative phenomenon. Consequently, the dissipation in the system causes the angular momentum hindrance during the fusion process. In this work, we have focused on the dissipative behavior of the fusing nuclei and its dependency on the incident energy. The dissipative evolution of the system depends not only on the entrance channel mass asymmetry but also on the incident energy, which was not mentioned in earlier studies. Moreover, the dissipative behavior of the fusing nuclei is also compared with respect to the entrance channel parameters like mass asymmetry $\alpha$ and the Coulomb interaction term $Z_P Z_T$. The dissipation phenomenon decreases when the mass asymmetry increases and it increases when the Coulomb interaction term $Z_P Z_T$ increases.

DOI: 10.1103/PhysRevC.98.024626

## I. INTRODUCTION

Heavy-ion fusion reactions are used to produce the composite nuclei with high excitation energy and angular momentum. The fusing nuclei disintegrate before the formation of a fully equilibrated compound nucleus (CN) or pre-equilibrium emission occurs if the projectile energy is above 10 MeV/nucleon; but at a low energy ($E/A < 10$ MeV), the pre-equilibrium contribution is only around 2–3% in the forward direction [1,2] and formation of CN becomes the dominant process. The hot and rotating CN decays through fission or emission of light particles such as $\alpha$, proton, neutron, and $\gamma$, leaving evaporation residue [3–6]. The higher angular momentum states decay preferentially through $\alpha$-particle emission or in the case of heavy CN, fission takes place, while the lower angular momentum states decay through proton or neutron emission. These emitted light particles carry important signatures about the underlying reaction mechanism of the fusion process. The statistical model has been used to explain the light particle evaporation spectra.

In earlier measurements, the charged-particle and neutron evaporation spectra are measured for the mass asymmetric and symmetric target-projectile systems. The charged-particle and neutron spectra are in agreement with the predictions of the statistical model in the case of asymmetric systems, but in the case of the symmetric systems, charged-particle and neutron spectra show deviations from the statistical model [7–12], as shown in Figs. 1 and 2. The exclusive neutron evaporation spectra measured for the asymmetric and symmetric systems show similar behavior as inclusive neutron evaporation spectra [13]. The charged-particle spectra are softer while the neutron spectra are harder with respect to the statistical model prediction for the symmetric systems.

To explain the deviation of the charged-particle spectra from the statistical model in the lower energy side, changes were required in the moment of inertia corresponding to the deformation [14], which indicates the dynamical effect in the de-excitation process for the charged-particle emission. The comparison of the decay time with the formation time of CN indicates that due to the presence of dissipation in the entrance channel, the formation time is comparable to the decay time in the case of the symmetric systems, which is not appropriate according to Bohr's hypothesis. So, it represents that the charged particles are emitted before the full relaxation of the compound nucleus [15]. It was also reported that there is a systematic change in the formation time of the compound nucleus and it gradually increases as we move from the asymmetric to the symmetric systems. The charged-particle spectra are affected by the entrance channel effect [16,17], where dissipation plays a pivotal role. Therefore, the statistical model, which considers that the formation time is much smaller than the decay time, over predicts the charged-particle evaporation spectra for symmetric systems [18]. The deviations of the charged-particle spectra from the statistical model predictions in the higher energy side are explained using the dynamical model calculation. The dynamical model suggests that due to the presence of the dissipative phenomenon in the entrance channel, the fusion of higher partial waves for the symmetric reactions is strongly hindered. The angular momentum value suggested by this model, which is less than the classical $l = l_{\max}$ explains the deviations for the $\alpha$-particle and proton spectra [8].

The anomalous deviation of the neutron evaporation spectra is explained using the higher value of the radius parameter $r_0$ and the smaller value of the level density parameter $a$. The higher value of $r_0$ enhances the available phase space and it increases the lower energy neutron yield, which affects the lower energy spectra. The excitation energy is related to the level density parameter by the relation $E = aT^2$, the smaller value of the level density parameter represents the

*nkrai233231@gmail.com

 

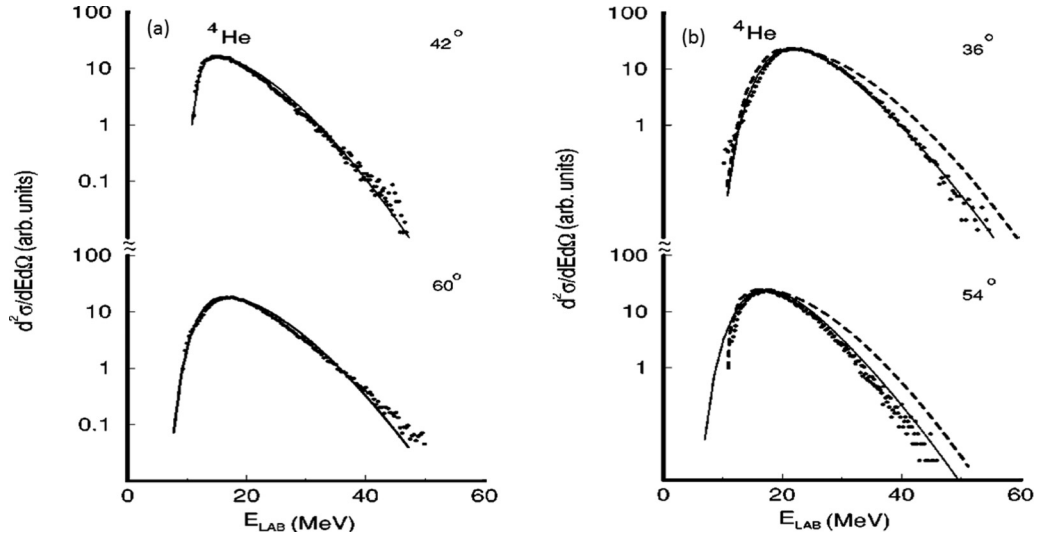


FIG. 1. Comparison of experimental charged-particle spectra (dots) with the statistical model (solid line) for asymmetric and symmetric reactions [7] (a) $^{16}O + ^{63}Cu$ at 109 MeV and (b) $^{34}S + ^{45}Sc$ at 140 MeV.

evaporation at the higher temperature from the compound nucleus populated by the symmetric systems, which affects the higher energy spectra. In symmetric systems, the formation time of CN was higher than in the asymmetric systems, which indicates that a temperature-equilibrated dinuclear complex system was formed that may be responsible for the neutron emission at a higher temperature [12]. But at the same time, it was found that thermal equilibrium is very fast, whereas the shape equilibrium is delayed [19].

Nuclear dissipation plays a crucial role in the low-energy heavy-ion fusion reactions. The angular momentum hindrance was present in the symmetric systems due to the dissipation in the entrance channel. Here, we have used the dynamical model to check whether the angular momentum hindrance is energy dependent or not, since the earlier measurements were done at fixed excitation energy for the symmetric and asymmetric systems. Therefore, we have chosen three asymmetric systems, $^{16}O + ^{64}Zn$, $^{12}C + ^{64}Zn$, and $^{12}C + ^{46}Ti$, and three symmetric systems, $^{31}P + ^{27}Al$, $^{32}S + ^{48}Ti$, and $^{28}Si + ^{27}Al$, to see the effect of energy variation on the dissipation phenomenon.

## II. DYNAMICAL MODEL

We have done the dynamical model calculation (HICOL), developed by the Feldmeier *et al.* [20], which is used to investigate the process of nuclear dissipation in the heavy-ion collision. The colliding nuclei are treated as two Fermi gases which may exchange particles, momentum, and entropy through the window. The time evolution of the collision trajectories is calculated by solving a Langevin equation with a fluctuating dissipative force. The nature of fluctuating force is determined from a microscopic picture of particle exchange between two colliding nuclei.

In the dynamical model, it is assumed that two spheres are connected by a conical neck and their dynamical evolution is represented by a sequence of shapes; and during the collision,

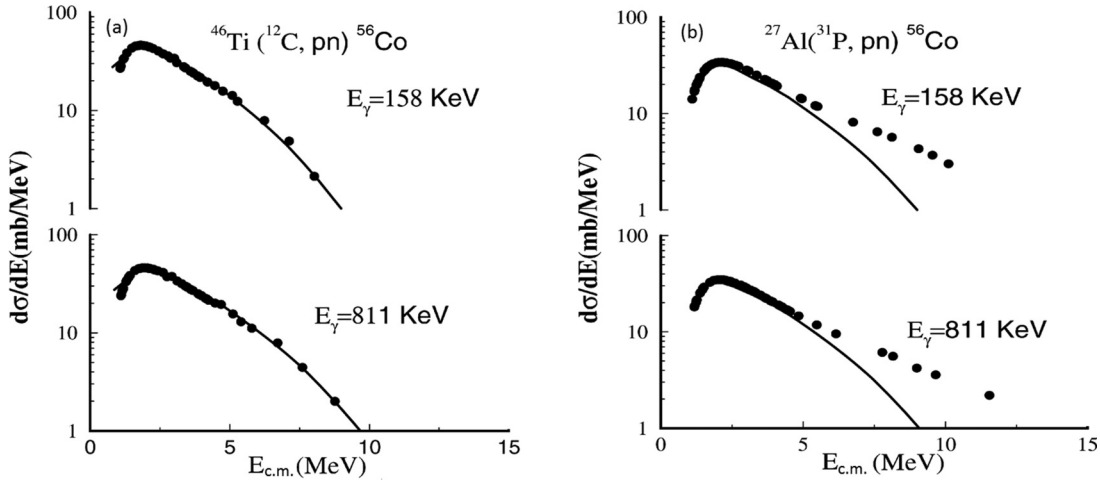


FIG. 2. Comparison of exclusive experimental neutron spectra (dots) with the statistical model (solid line) for asymmetric reaction and symmetric reactions [13] (a) $^{12}C + ^{46}Ti$ at 80 MeV and (b) $^{31}P + ^{27}Al$ at 131 MeV.

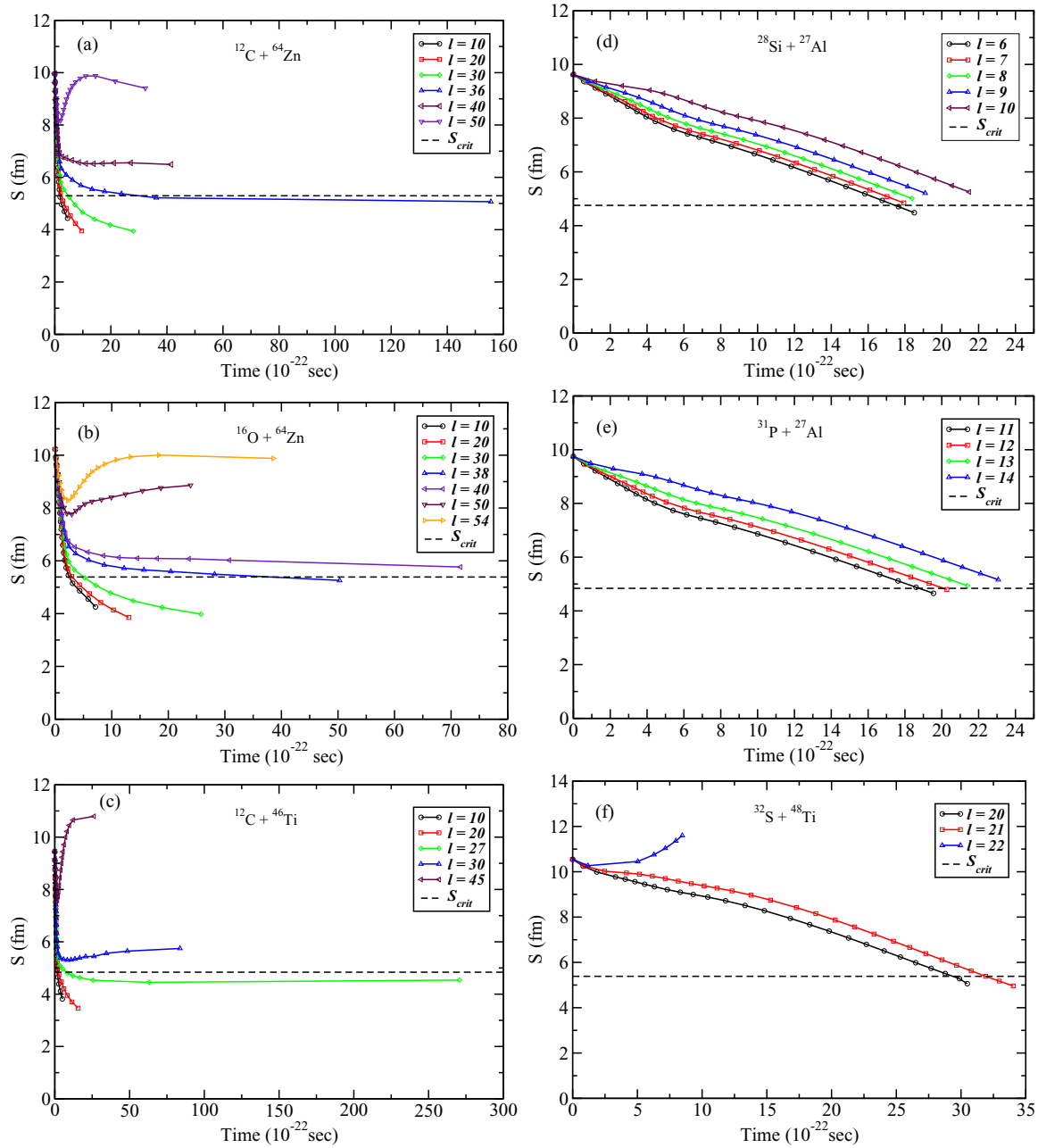


FIG. 3. Calculated evolution of the separation ($s$) as a function of time for asymmetric systems (a)–(c) and symmetric systems (d)–(f).

the mass and charged density remain constant by conserving the volume of shape. The axially symmetric configurations with sharp surfaces represent the macroscopic shapes of the nuclear system. The shapes of evolving nuclei are uniquely determined by three macroscopic degrees of freedom: the distance between the nuclei ($s$) elongation, the neck coordinate ($\sigma$), and the asymmetry coordinate ($\Delta$), defined as

$$s = \text{distance between two spheres},$$

$$\sigma = \frac{V_o - \left(\frac{4\pi}{3}\right)R_1^3 - \left(\frac{4\pi}{3}\right)R_2^3}{V_o} = \frac{\text{neck volume}}{\text{total volume}},$$

$$\Delta = \frac{R_1 - R_2}{R_1 + R_2} = \text{asymmetry},$$

where $V_o$ is the total volume of the system and it is independent of $s$, $\sigma$, and $\Delta$. $R_1$ and $R_2$ are the radii of the two interacting nuclei. In addition to the three shape degrees of freedom, there are three rotational degrees of freedom for the intrinsic and relative rotation of the dinuclear complex. Denoting the six macroscopic coordinates and their momenta by $[q(t), p(t)]$, the Langevin dynamical equations of motion can be written as

$$\frac{d\mathbf{p}}{dt} = -\frac{dT}{dq} - \frac{dV}{dq} + X(t),$$

$$\frac{d\mathbf{q}}{dt} = M^{-1}p,$$

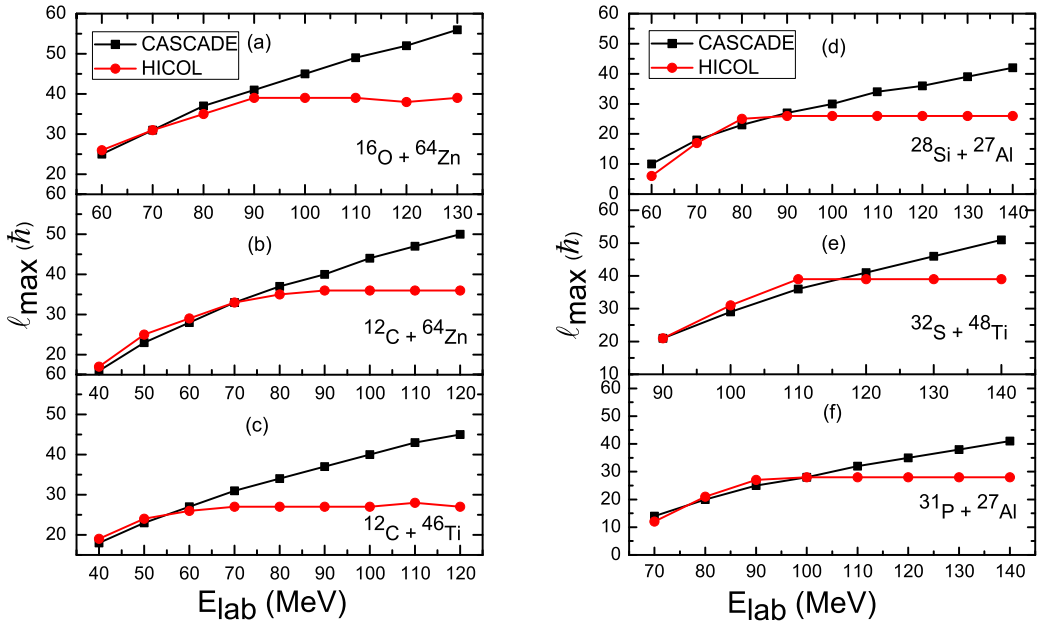


FIG. 4. Variation of angular momentum $l_{max}$ with respect to incident energy $E_{lab}$ for asymmetric systems (a)–(c) and symmetric systems (d)–(f).

where $T$ denotes the collective kinetic energy and $M$ denotes the mass tensor, while $V$ stands for the conservative potential and $X(t)$ is the fluctuating force caused by the coupling of the collective degrees of freedom to the intrinsic degrees of freedom. The collective kinetic energy can be written as

$$T = \frac{1}{2}\sum_{i,j=1}^{6} M_{ij}\dot{q}_i\dot{q}_j.$$

The mass tensor is calculated from the profile function by assuming incompressible and irrotational flow of mass during the shape evolution in the collision. The expression of the mass parameters related to profile functions is given by Feldmeier *et al.* [20]. The potential energy $V$ is calculated by associating with each shape the nuclear and Coulomb energies. The nuclear potential $V_n$ is obtained as a double volume integral of a Yukawa plus exponential folding function,

$$V_n = \frac{-c_s}{8\pi^2 r_o^2 a^3}\int_{\text{shape}} d^3r\,d^3r'\left(\frac{1}{a}-\frac{2}{|r-r'|}\right) \times \exp\left(-\frac{|r-r'|}{a}\right).$$

The parameters are from Krappe *et al.* [21], where

$$c_s = a_s\left[1-\kappa_s\left(\frac{N-Z}{A}\right)^2\right] \quad a_s = 21.7\ \text{MeV}, \quad \kappa_s = 3,$$

$$r_o = 1.18\ \text{fm} \quad a = 0.65\ \text{fm}.$$

The Coulomb potential $V_c$ is calculated assuming a uniform charge distribution $\rho_c$ with a sharp surface.

$$V_c = \frac{1}{2}\rho_c^2\int_{\text{shape}} d^3r\,d^3r'\frac{1}{|r-r'|}.$$

The total potential energy is the sum of the nuclear and Coulomb parts,

$$V(s,\sigma,\Delta) = V_n + V_c.$$

The motion of the system is governed by strong a dissipative force $X(t)$, which is related to the friction and the diffusion terms obtained from the particle exchange model [22]. The one-body dissipation is considered to be predominant because it has been found to be more relevant for this type of reaction [23]. In this model, a realistic macroscopic description of the nucleus-nucleus collision is considered, which is based on the concept of one-body dissipation. This model consistently describes the dynamical evolution of various composite systems formed in nucleus-nucleus collisions in a wide range of impact parameters.

## III. RESULTS AND DISCUSSIONS

We have carried out the HICOL calculations for the three asymmetric systems $^{16}O + ^{64}Zn$, $^{12}C + ^{64}Zn$, and $^{12}C + ^{46}Ti$ and for the three symmetric systems $^{31}P + ^{27}Al$, $^{32}S + ^{48}Ti$, and $^{28}Si + ^{27}Al$. The distance between the fusing nuclei $s$ is plotted as a function of time for the various values of $l$ for both symmetric and asymmetric systems, which is shown in Fig. 3. In Fig. 3, going downward, the mass asymmetry decreases in the left column, while in the right column mass asymmetry increases. The dashed line corresponds to the closest distance of approach, $s = s_{crit}$, which is taken as equal to the radius of the CN, $R = r_o A^{1/3}$; the plots show that for each system the trajectories up to $l > l_{max}$ do not approach $s = s_{crit}$ and hence only the partial waves up to $l = l_{max}$ fuse into the CN.

We have calculated the angular momentum by the dynamical model and the statistical model by changing the projectile energy for both the symmetric and asymmetric systems and the results are plotted in Fig. 4. The angular momentum

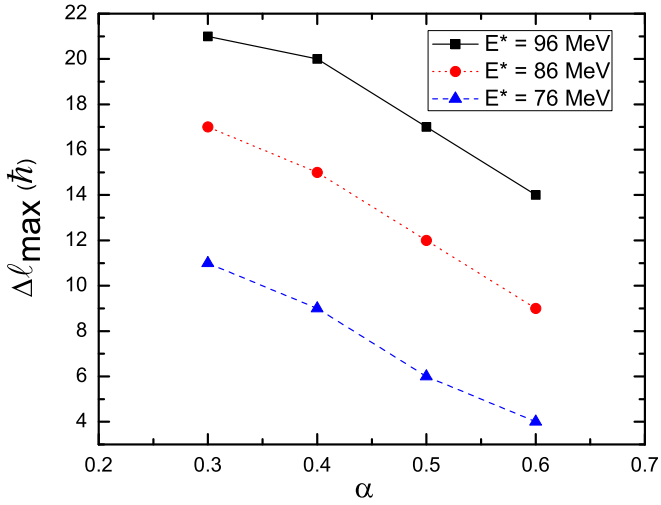


FIG. 5. Variation of angular momentum difference $\Delta l_{max}$ with respect to mass asymmetry $\alpha$ for various target-projectile combinations, leading to the same compound nucleus $^{80}$Sr at different excitation energies.

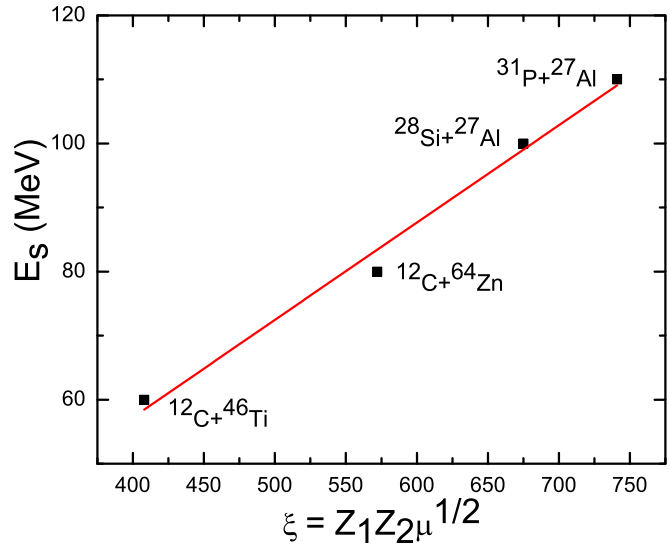


FIG. 7. Threshold energy $E_s$ vs $\zeta$ for several heavy-ion fusion systems, where the $Q$ values for the fusion are positive.

calculated by the statistical model calculation (CASCADE) [24] is the CN angular momentum, while HICOL-predicted angular momentum is that angular momentum which is contributing to the fusion. It indicates that for the particular reaction, the whole angular momentum as calculated by the statistical model calculation (CASCADE) does not contribute to the fusion; what causes the angular momentum hindrance is indicated by the dynamical model calculation (HICOL) and it indicates that the increase in the hindrance is directly proportional to the incident energy of the projectile.

To understand how $\Delta l_{max}$ (angular momentum hindrance) depends on the entrance channel mass asymmetry [$\alpha = (A_T - A_P)/(A_T + A_P)$], we have calculated $\Delta l_{max}$ for the

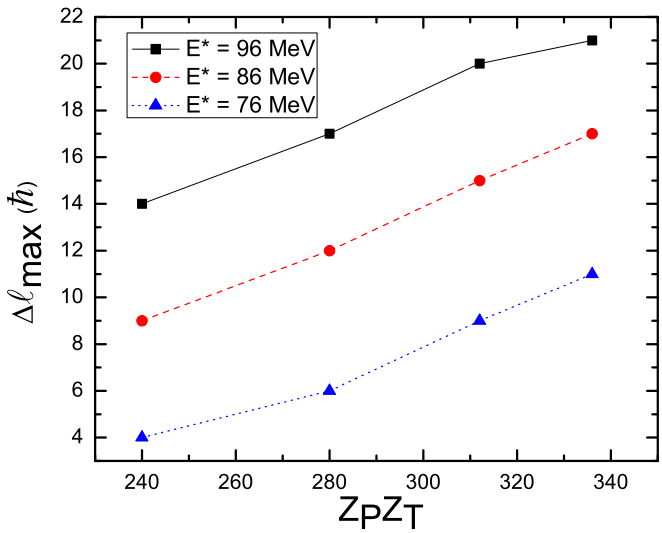


FIG. 6. Variation of angular momentum difference $\Delta l_{max}$ with respect to the charge product $Z_P Z_T$ for various target-projectile combinations, leading to the same compound nucleus $^{80}$Sr at different excitation energies.

combination of some symmetric as well as asymmetric systems. The systems are like $^{28}$Si + $^{52}$Cr, $^{24}$Mg + $^{56}$Fe, $^{20}$Ne + $^{60}$Ni, and $^{16}$O + $^{64}$Zn, leading to the same compound nucleus $^{80}$Sr at the different excitation energies. The variation of $\Delta l_{max}$ with respect to mass asymmetry $\alpha$ is shown in Fig. 5. It was observed in Fig. 5 that the $\Delta l_{max}$ almost linearly decreases with the increase in their mass asymmetry, while the value of $\Delta l_{max}$ increases with increasing excitation energy as shown in Fig. 4.

In another study, the $\Delta l_{max}$ was also compared in terms of the charge product of the projectile and target $Z_P Z_T$, where $Z_P$ and $Z_T$ are the atomic numbers of the projectile and target nuclei, respectively. For this work, we have chosen the four target-projectile combinations $^{28}$Si + $^{52}$Cr, $^{24}$Mg + $^{56}$Fe, $^{20}$Ne + $^{60}$Ni, and $^{16}$O + $^{64}$Zn, leading to the same compound nucleus $^{80}$Sr at different excitation energies and $\Delta l_{max}$ is plotted as a function of $Z_P Z_T$ at a constant excitation energy in Fig. 6. It can be seen from Fig 6 that $\Delta l_{max}$ has a linear growth when the charge product $Z_P Z_T$ increases. But the overall $\Delta l_{max}$ increases with the excitation energy. Hence, it can be pointed out that as the projectile approaches the target nucleus, the Coulomb interaction increases, which results in the increase of $\Delta l_{max}$.

In Refs. [25,26], it was pointed out that in the light-medium mass nuclei with positive $Q$ values for fusion, the threshold energy $E_s$ for the fusion hindrance is a function of the entrance channel parameter $\zeta = Z_1 Z_2 \sqrt{\mu}$, where $\mu = A_1 A_2/(A_1 + A_2)$. Here, we now apply this phenomenon to the systems with the positive $Q$ values: $^{12}$C + $^{46}$Ti, $^{12}$C + $^{64}$Zn, $^{28}$Si + $^{27}$Al, and $^{31}$P + $^{27}$Al, the $E_s$ follows the same trend as mentioned in Refs. [25,26], which is shown in Fig. 7.

## IV. CONCLUSION

In this work, we have observed that the angular momenta calculated by the statistical model calculation (CASCADE) and

the dynamical model calculation (HICOL) suggest different values of the angular momentum contribution in the higher energy region compared to the lower energy region for both symmetric and asymmetric systems. The angular momentum hindrance ($\Delta l_{\max}$) increases with the incident energy of the projectile for both symmetric and asymmetric systems, from which we conclude that the dissipation in the entrance channel increases with the projectile energy and causes the angular momentum hindrance in both the symmetric and asymmetric systems at the higher energy. Moreover, the dissipative behavior of the fusing nuclei is also compared with respect to the entrance channel parameters like mass asymmetry $\alpha$ and the Coulomb interaction term $Z_P Z_T$ at constant excitation energy and we observed that with increasing value of mass asymmetry it decreases almost linearly and it increases almost linearly when the Coulomb interaction term $Z_P Z_T$ increases. The threshold energy $E_s$ for the fusion hindrance was found to be in good agreement with the phenomenological estimate of Refs. [25,26]. So it is desirable to perform more experiments of this kind to verify the above-mentioned results for both symmetric and asymmetric systems.

## ACKNOWLEDGMENTS

One of the authors (A.K.) thanks the IUAC-UGC, Government of India (Sanction No. IUAC/XIII.7/UFR-58310), DST, Government of India (Sanction No. INT/RUS/RFBR/P-250), and DAE-BRNS, Government of India (Sanction No. 36(6)/14/23/2016-BRNS) for the financial support for this work.

[1] S. Paul, C. Sunil, Sanjoy Pal, V. Nanal, V. Suman, G. S. Sahoo, A. Shanbhag, S. P. Tripathy, T. Bandyopadhyay, M. Nandy, and A. K. Mohanty, Phys. Rev. C **96**, 044607 (2017).
[2] S. Paul, M. Nandy, A. K. Mohanty, and Y. K. Gambhir, Phys. Rev. C **94**, 034607 (2016).
[3] B. Fornal, G. Viesti, G. Nebbia, G. Prete, and J. B. Natowitz, Phys. Rev. C **40**, 664 (1989).
[4] R. J. Charity, Phys. Rev. C **82**, 014610 (2010).
[5] S. Kundu, C. Bhattacharya, S. Bhattacharya, T. K. Rana, K. Banerjee, S. Muhkopadhayay, D. Gupta, A. Dey, and R. Saha, Phys. Rev. C **87**, 024602 (2013).
[6] A. Gavron, J. R. Beene, R. L. Ferguson, F. E. Obenshain, F. Plasil, G. R. Young, G. A. Petitt, K. G. Young, M. Jääskeläinen, D. G. Sarantites, and C. F. Maguire, Phys. Rev. C **24**, 2048 (1981).
[7] J. Kaur, I. M. Govil, G. Singh, Ajay Kumar, A. Kumar, B. R. Behera, and S. K. Datta, Phys. Rev. C **66**, 034601 (2002).
[8] J. Kaur, A. Kumar, Ajay Kumar, G. Singh, S. K. Datta, and I. M. Govil, Phys. Rev. C **70**, 017601 (2004).
[9] B. Fornal, F. Gramegna, G. Prete, G. Nebbia, R. Smith, G. D'Erasmo, L. Fiore, A. Pantaleo, G. Viesti, P. Blasi, F. Lucarelli, I. Iori, and A. Moroni, Phys. Rev. C **41**, 127 (1990).
[10] I. M. Govil, Pramana - J. Phys. **53**, 381 (1999).
[11] A. Kumar, A. Kumar, G. Singh, B. K. Yogi, R. Kumar, S. K. Datta, M. B. Chatterjee, and I. M. Govil, Phys. Rev. C **68**, 034603 (2003).
[12] Ajay Kumar, A. Kumar, G. Singh, Hardev Singh, R. P. Singh, Rakesh Kumar, K. S. Golda, S. K. Datta, and I. M. Govil, Phys. Rev. C **70**, 044607 (2004).
[13] A. Kumar, H. Singh, R. Kumar, I. M. Govil, R. P. Singh, Rakesh Kumar, B. K. Yogi, K. S. Golda, S. K. Datta, and G. Viesti, Nucl. Phys. A **798**, 1 (2008).
[14] D. K. Agnihotri, A. Kumar, K. C. Jain, K. P. Singh, G. Singh, D. Kabiraj, D. K. Avasthi, and I. M. Govil, Phy. Lett. B **307**, 283 (1993).
[15] I. M. Govil, R. Singh, A. Kumar, J. Kaur, A. K. Sinha, N. Madhavan, D. O. Kataria, P. Sugathan, S. K. Kataria, K. Kumar, Bency John, and G. V. Ravi Prasad, Phys. Rev. C **57**, 1269 (1998).
[16] A. Shamlath, E. Prasad, N. Madhavan, P. V. Laveen, J. Gehlot, A. K. Nasirov, G. Giardina, G. Mandaglio, S. Nath, T. Banerjee, A. M. Vinodkumar, M. Shareef, A. Jhingan, T. Varughese, D. Kumar, P. S. Devi, Khushboo, P. Jisha, Neeraj Kumar, M. M. Hosamani, and S. Kailas, Phys. Rev. C **95**, 034610 (2017).
[17] A. Shrivastava, K. Mahata, S. K. Pandit, V. Nanal, T. Ichikawa, K. Hagino, A. Navin, C. S. Palshetkar, V. V. Parkar, K. Ramachandran, P. C. Rout, A. Kumar, A. Chatterjee, and A. Chatterjee, Phy. Lett. B **755**, 332 (2016).
[18] I. M. Govil, R. Singh, A. Kumar, Ajay Kumar, G. Singh, S. K. Kataria, and S. K. Datta, Phys. Rev. C **62**, 064606 (2000).
[19] M. Kaur, B. R. Behera, G. Singh, V. Singh, R. Sandal, A. Kumar, H. Singh, G. Singh, K. P. Singh, N. Madhavan, S. Nath, A. Jhingan, J. Gehlot, K. S. Golda, P. Sugathan, D. Siwal, S. Kalkal, E. Prasad, and S. Appannababu, Phys. Rev. C **89**, 034621 (2014).
[20] H. Feldmeier, Rep. Prog. Phys **50**, 915 (1987).
[21] H. J. Krappe, J. R. Nix, and A. J. Sierk, Phys. Rev. C **20**, 992 (1979).
[22] H. Feldmeier and H. Spangenberger, Nucl. Phys. A **435**, 229 (1985).
[23] J. Blocki, R. Planeta, J. Brzychczyk, and K. Grotowski, Z. Phys. A **341**, 307 (1992).
[24] F. Puhlhofer, Nucl. Phys A **280**, 267 (1977).
[25] C. L. Jiang, K. E. Rehm, B. B. Back, and R. V. F. Janssens, Phys. Rev. C **79**, 044601 (2009).
[26] G. Montagnoli, A. M. Stefanini, C. L. Jiang, K. Hagino, F. Galtarossa, G. Colucci, S. Bottoni, C. Broggini, A. Caciolli, P. Colovic, L. Corradi, S. Courtin, R. Depalo, E. Fioretto, G. Fruet, A. Gal, A. Goasduff, M. Heine, S. P. Hu, M. Kaur, T. Mijatovic, M. Mazzocco, D. Montanari, F. Scarlassara, E. Strano, S. Szilner, and G. X. Zhang, Phys. Rev. C **97**, 024610 (2018).